JOURNAL OF CATALYSIS **179,** 192–202 (1998)
ARTICLE NO. CA982177

Structure and Density of Active Zn Species in Zn/H-ZSM5 Propane Aromatization Catalysts

Joseph A. Biscardi,* George D. Meitzner,† and Enrique Iglesia*,[1]

*Department of Chemical Engineering, University of California, Berkeley, Berkeley, California 94720; and †Edge Analytical P.O. Box 2365, Stanford, California 94309

Received January 21, 1998; revised June 3, 1998; accepted June 4, 1998

Exchanged Zn cations increase propane conversion turnover rates, hydrogen formation rates, and selectivity to aromatics on H-ZSM5. *In situ* **Zn** *K***-edge X-ray absorption studies show that aqueous ion exchange with H-ZSM5 (Si/Al = 14.5) leads to isolated Zn^{2+} cations with tetrahedral symmetry. These Zn species reside at cation exchange sites as monomeric cations and form directly from nitrate solutions during ion exchange. X-ray absorption and temperature-programmed reduction studies show that Zn^{2+} cations in Zn/H-ZSM5 do not reduce to zero-valent species during propane reactions at 773 K. Extrazeolitic ZnO crystals form on samples prepared by impregnation techniques. In contrast to exchanged Zn^{2+} cations, these bulk ZnO crystals reduce to Zn metal and elute from the catalyst bed as Zn vapor under typical propane aromatization conditions. Condensation reactions of $(Zn^{2+}OH)^+$ species with acidic OH groups appear to lead to the formation of the active Zn^{2+} cations interacting with two Al sites (O^-–Zn^{2+}–O^-). This active Zn species is supported by acid site density measurements from NH_3 titration and isotopic titration of remaining Brønsted acid sites with deuterium in Zn/H-ZSM5.** © 1998 Academic Press

1. INTRODUCTION

H-ZSM5 catalyzes the conversion of light alkanes to aromatics with low selectivity because of cracking side reactions (1–7). The introduction of Zn species into H-ZSM5 increases the rate and selectivity of aromatization reactions (8–17). These metal cations increase propane conversion rates and the selectivity to unsaturated products by increasing the rate of propane and propene dehydrogenation and by avoiding the preferential removal of hydrogen by transfer to hydrocarbon fragments to form light alkanes.

Many groups have examined the catalytic role of these Zn species during light alkane aromatization; the structure and location of these Zn cations in Zn/H-ZSM5, however, were not explored until recently. Structural studies of Zn species in Zn/H-ZSM5 have led to conflicting reports. Yakerson *et al.* (18) concluded from infrared studies of pyridine adsorbed on Zn/H-ZSM5 (<2 wt% Zn, Si/Al = 15) that one Zn^{2+} cation replaces two protons and interacts with two aluminum sites (O^-–Zn–O^-). In contrast, Berndt *et al.* (16) showed that CO reacts on Zn/H-ZSM5 (<2 wt% Zn, Si/Al = 23) to produce equimolar amounts of CO_2 and H_2, suggesting that $(ZnOH)^+$ is present.

This study addresses the synthesis of Zn cation-exchanged H-ZSM5 zeolite and the detailed characterization of the structure and location of the Zn species. The nature of Zn species in Zn/H-ZSM5 was examined by combining site titration and kinetic and isotopic methods with *in situ* X-ray absorption spectroscopy at the Zn *K*-edge.

2. EXPERIMENTAL CONDITIONS

2.1. Catalyst Preparation

Na^+ ions in Na-ZSM5 (Zeochem) were replaced with NH_4^+ by contacting the Na-ZSM5 with a solution of 0.67 M NH_4NO_3 (Fisher, Certified ACS, >98.0%) at 353 K for 10 h. Solids were separated from the solution by filtering. The exchange procedure was repeated three times using fresh NH_4NO_3 solutions to ensure complete exchange of Na cations. The residual Na content was less than 0.07 wt% by atomic absorption analysis. Catalyst samples were then dried in flowing air at 383 K for 20 h and treated in flowing dry air at 773 K for 20 h to decompose NH_4^+ to H^+ and to form the acidic form of the zeolite (H-ZSM5). Three Zn/H-ZSM5 catalysts were prepared by ion exchange at 343 K for 1, 5.5, or 9 h using H-ZSM5 and a solution of $Zn(NO_3)_2$ (0.0050 M, Aldrich, >98.0%). The exchanged Zn/H-ZSM5 samples were then dried in flowing air at 383 K for 20 h and treated in flowing dry air at 773 K for 20 h. Zn/H-ZSM5 was also prepared by incipient wetness impregnation using a $Zn(NO_3)_2$ solution (0.0050 M, Aldrich, >98.0%). This impregnated Zn/H-ZSM5 sample was dried in flowing air at 383 K for 20 h and treated in flowing dry air at 773 K for 20 h.

2.2. Elemental Analysis

The elemental composition of all samples was obtained by atomic absorption spectroscopy (Galbraith

[1] To whom correspondence should be addressed. Fax: (510) 642–4778. E-mail: iglesia@cchem.berkeley.edu.

0021-9517/98 $25.00

Laboratories). The atomic Si/Al ratio in all samples was 14.5 ± 0.9. The Zn contents of the ion-exchanged samples were 0.62, 1.07, and 1.30 wt%, which correspond to Zn/Al atomic ratios of 0.10, 0.16, and 0.19 respectively. The Zn content of the impregnated sample was 2.80 wt% ($Zn/Al = 0.40$).

2.3. *In Situ Zinc K-Edge X-ray Absorption Spectroscopy*

The structure and chemical state of Zn species in Zn/H-ZSM5 samples were determined by *in situ* X-ray absorption at the Zn *K*-edge, using beamline 4-1 at the Stanford Synchrotron Research Laboratory (SSRL). This beamline uses an unfocused Si (220) double-crystal, parallel geometry, upward reflecting monochromator. The intensity of the incident and transmitted X-rays was recorded using three Ar-purged ionization chambers. An accurate energy calibration of the X-ray spectra was achieved by measuring simultaneously data from Zn/H-ZSM5 and from a reference sample (ZnO) located between the second and third ionization chambers.

X-ray absorption measurements were conducted using an *in situ* cell similar to that described by Clausen *et al.* (19). The cell consists of a quartz capillary (0.9-mm diameter, 0.1-mm wall thickness, 10-cm length) mounted horizontally into a stainless-steel base using compression fittings with graphite ferrules. Samples with 45- to 60-mesh particle sizes formed a dense bed through which gas flows with negligible pressure drop. Heat was supplied by four heat cartridges mounted into a copper block with ten fins and a slit for the sample and the X-ray beam. Temperature uniformity was ensured by measuring the temperature profile along the capillary under conditions identical to those of the *in situ* experiments.

Gases were introduced into the X-ray absorption cell using a portable gas handling unit and He, H_2, and propane lecture bottles. Helium (Matheson, chemical purity >99.995%) and propane (Matheson, chemical purity >99.5%) were purified using a water trap (Oxyclear, 5A) followed by an oxygen indicating trap (Matheson, Oxisorb), both held at room temperature. Hydrogen (Matheson, chemical purity >99.99%) was purified by passing through a catalytic purifier (Matheson) and then through a water removal trap (Oxyclear, 5A). After purification, gas flow rates were controlled by an electronic mass flow meter (Porter Instrument Co.), and then further purified by an additional oxygen indicating trap (Matheson, Oxisorb) before entering the sample cell.

Zn *K*-edge spectra were analyzed by setting the edge energy at the first inflection point in the edge region. The pre-edge region of the spectrum was then fitted by a straight line. A polynomial spline with seven nodes was used to describe the high-energy side of the edge ($\Delta E = 10$–1000 eV). Both the pre-edge and post-edge functions were extrapolated to the absorption edge energy and the entire spectrum was normalized by the height of the resulting absorbance step at the edge. The near-edge (XANES) and extended fine-structure (EXAFS) spectra were obtained by subtracting the pre-edge and post-edge fitting functions from the raw absorption data.

2.4. *Temperature-Programmed Reduction*

Temperature-programmed reduction experiments were carried out using a Quantasorb unit (Quantachrome) modified with a programmable furnace. Samples were held within a quartz cell containing a thermowell in direct contact with the sample bed. The samples were flushed with N_2 (Matheson, chemical purity >99.998%, 50 cm^3/min) at room temperature for 0.5 h before reduction. The reduction was conducted by flowing a H_2/Ar mixture (21.0%, Matheson, certified standard, 80 cm^3/min) through the samples with flow rates measured by an electronic mass flowmeter (Porter Instrument Co.). The sample exit stream was passed through a molecular sieve trap (Aldrich Chemicals, 13X) to remove water before thermal conductivity measurements. The inlet and outlet streams were passed through a thermal conductivity detector (TCD). The temperature and TCD signals were recorded using Labview software. The temperature was increased at 10 K/min from room temperature to 1073 K. The TCD output was calibrated using a WO_3 standard (Aldrich, 99.99%, treated in O_2 for 3 h at 973 K). H_2 consumption rates were normalized by the amount of Zn present and plotted versus the measured temperature.

2.5. *Measurement of Ammonia Irreversibly Adsorbed at 383 K*

Ammonia titration experiments were carried out using a temperature-programmed surface reaction (TPSR) unit consisting of a gas manifold unit connected to a quartz capillary cell followed by an on-line mass spectrometer. Samples were charged into the capillary cell, purged with helium (Matheson, >99.999%, 100 cm^3/min) at 773 K for 1 h, and cooled to 383 K. A mixture of NH_3/He (0.93% NH_3, Matheson, certified standard, 80 cm^3/min) was passed through the sample for 0.4 h or until NH_3 levels reached a constant value in the effluent stream. Once titrations were complete, He flow (100 cm^3/min) for about 3 h was used to remove physisorbed NH_3. Temperature-programmed desorption is carried out by increasing the temperature from 383 to 1000 K at 15 K/min. The NH_3 concentration in the effluent gas was measured continuously using a mass spectrometer (Leybold–Inficon, Model THP TS200).

2.6. *Isotopic Titration of Brønsted Acid Sites with Deuterium*

Isotopic titration experiments were also carried out using the TPSR unit. Samples were charged into a capillary quartz cell, heated to 773 K in a flowing H_2/Ar mixture

(5% H_2, Matheson, certified standard, 100 cm^3/min), held isothermal for 2 h, and then cooled to 300 K. The flow was then switched to a D_2/Ar mixture (5% D_2, Matheson, certified standard, 100 cm^3/min) and the temperature was increased from 300 to 1073 K at 15 K/min. The H_2, HD, and D_2 concentrations in the effluent were measured by mass spectrometry.

2.7. Catalytic Reaction Studies

Kinetic studies on H-ZSM5 and Zn/H-ZSM5 catalysts were performed in a gradientless recirculating reactor operated in the batch mode. This reactor system was used to measure the chemical composition of reaction products as a function of reaction time and reactant conversion. The reaction mixture was circulated using a graphite gear micropump (250 cm^3 min^{-1}, Cole-Parmer) that allowed differential reactor operation (<2% reactant conversion per pass).

The chemical composition of reaction mixtures was obtained using capillary column gas chromatography with flame ionization detection (Hewlett–Packard 5890, HP-1 methyl-silicone column, 50 m, 0.32-mm diameter, 1.05-μm film thickness). Propane (Matheson, chemical purity >99.5%) was used without further purification. Helium (Linde, chemical purity >99.995%) was purified by passage through oxygen removal (Matheson, Oxisorb) and molecular sieve (13X and 5A) traps at room temperature. Helium was used as an inert diluent in most of the catalytic studies.

Batch reactor data are shown as product site yields (molecules of product per Al site) or reactant turnovers (molecules of C_3H_8 converted per Al site) as a function of contact time. The slope of these plots gives the propane conversion turnover rate or product site-time yield. Hydrocarbon selectivities are reported on a carbon basis as the percentage of the converted propane that appears as each reaction product. Hydrogen selectivities are reported as the percentage of the hydrogen atoms in the converted propane that appears within a given hydrocarbon product or as H_2.

3. RESULTS AND DISCUSSION

3.1. Effect of Zn Metal Cations on Propane Conversion Rate and Selectivity

Propane conversion turnover rates are greater on Zn/H-ZSM5 than on H-ZSM5 (Fig. 1). When Zn cations are introduced into H-ZSM5 channels, dehydrogenated products are produced with higher selectivity and the rate of formation of aromatics increases markedly (Table 1). The selectivity to C_6+ aromatics at similar conversions (7.6–8.3%) increases from 2.4% to 35.4% when Zn (1.30 wt%) is ion-exchanged into H-ZSM5. Aromatic site-time yields increase monotonically with increasing Zn content (0–1.30 wt%) (Fig. 2).

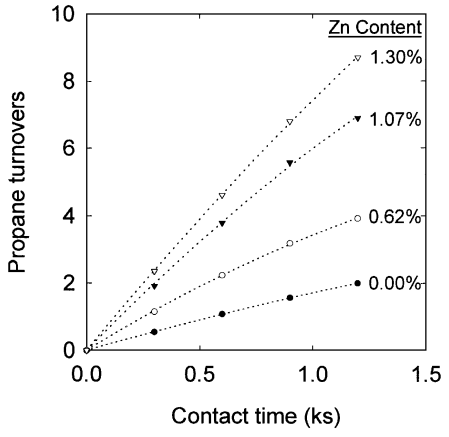

FIG. 1. Propane turnovers versus contact time during propane conversion on H-ZSM5 and Zn/H-ZSM5 (773 K, 26.6 kPa C_3H_8, 74.7 kPa He).

The presence of Zn species leads to an increase in the rate of H_2 formation. The hydrogen (H_2) selectivity increases with increasing Zn content (Fig. 3). On H-ZSM5, H_2 selectivity remains low (4–6%) at all conversions, but the addition of Zn (1.30 wt%) increases hydrogen selectivity (30–31%) (Table 1). On all Zn/H-ZSM5 catalysts, hydrogen selectivity is independent of propane conversion.

Kinetic studies indicate that propane conversion to aromatics requires sequential dehydrogenation steps and acid-catalyzed reactions of propene intermediates (6,7). Propane dehydrogenation reactions proceed via elementary steps that involve C–H bond activation and disposal of hydrogen atoms formed in these reactions. Hydrogen removal can occur via bimolecular or surface-mediated

TABLE 1

Propane Turnover Rates and Product Distribution on H-ZSM5 and Zn/H-ZSM5 (773 K, 26.6 kPa C_3H_8, 74.7 kPa He)

	Zn (wt%)			
	0.00	0.62	1.07	1.30
Zn/Al	0.00	0.10	0.16	0.19
Propane conversion (%)	7.6	7.7	7.6	8.3
Propane turnover rate (per Al, 10^{-3} s^{-1})	1.7	2.5	4.7	5.1
Carbon selectivity (%)				
Methane	23.2	11.5	7.0	6.2
Ethene	33.2	23.3	14.9	14.6
Ethane	7.3	3.1	6.2	4.1
Propene	22.4	29.0	33.7	34.7
C_6^+ aromatics	2.4	28.3	33.5	35.4
Benzene	0.8	12.4	15.2	15.4
Toluene	1.5	11.1	13.0	14.0
C_8^+	0.1	4.8	5.3	6.0
Hydrogen selectivity (%)				
Hydrogen (H_2)	4.6	25.2	29.0	31.0

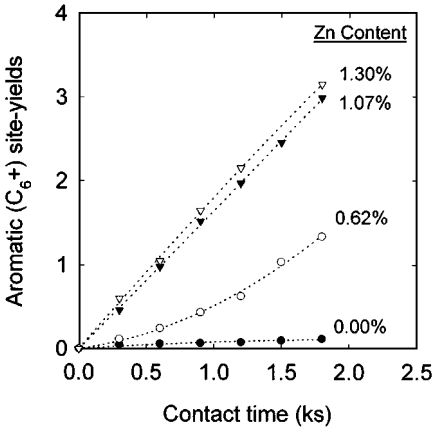

FIG. 2. Aromatic (C_6+) site yields versus contact time during propane conversion on H-ZSM5 and Zn/H-ZSM5 (773 K, 26.6 kPa C_3H_8, 74.7 kPa He).

transfer to adsorbed hydrocarbons or by recombinative desorption to form H_2. Isotopic exchange experiments show that these C–H bond activation steps are quasi-equilibrated and that hydrogen removal limits aromatization rates and selectivity on H-ZSM5 (12–14,17). The presence of exchanged Zn cations increases the rate of these hydrogen removal steps by introducing "portholes" for recombinative desorption of H atoms as H_2 (14). Exchanged Zn cations increase the rates of propane conversion to aromatics, of recombinative hydrogen desorption, and of incorporation of D atoms from D_2 into reaction products (14).

3.2. X-ray Absorption Zn K-Edge Near-Edge Spectra

Near-edge X-ray absorption spectra at the Zn *K*-edge for fresh Zn/H-ZSM5 at room temperature show a sharp increase in absorbance (edge energy) at 9664 eV, caused by the excitation of Zn 1*s* electrons. The edge energy depends

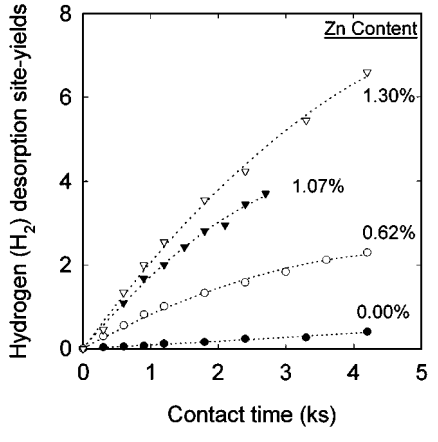

FIG. 3. Hydrogen (H_2) desorption site yields versus contact time during propane conversion on H-ZSM5 and Zn/H-ZSM5 (773 K, 26.6 kPa C_3H_8, 74.7 kPa He).

TABLE 2

Absolute Absorption Edge Energies at the Zn *K*-Edge for Zn Foil, ZnO, and Zn/H-ZSM5 (293 K)

Sample	Oxidation state	Edge energy (eV)
Zn foil	Zn^0	9659
ZnO	Zn^{2+}	9664
1.07% Zn/H-ZSM5	Zn^{2+}	9664
1.30% Zn/H-ZSM5	Zn^{2+}	9664

All samples as received; the positions of the edges are defined by the first inflection points.

on the oxidation state of the absorber atom (20); absorption edges shift to higher energy during oxidation. Standard Zn compounds (Zn foil and ZnO) were used to determine the oxidation state of the Zn in Zn/H-ZSM5. The Zn *K*-edge energy of Zn foil (Zn^0) was measured at 9659 eV and that for ZnO (Zn^{2+}) at 9664 eV (Table 2). Near-edge spectra of fresh Zn/H-ZSM5 show that Zn species have absorption energies similar to that in ZnO, suggesting that they consist of Zn^{2+} cations.

The normalized near-edge spectrum (−30 to 60 eV from the absorption edge) of a fresh 1.07% Zn/H-ZSM5 sample is shown in Fig. 4. The edge energy is not affected by mild thermal treatment (323 K in He, H_2, or C_3H_8), but the

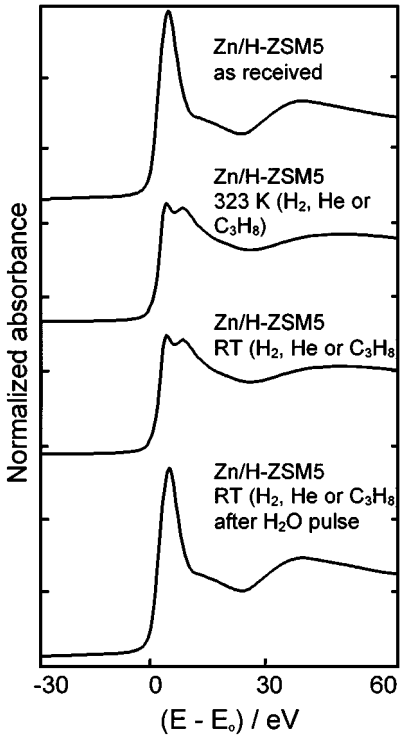

FIG. 4. Normalized Zn *K*-edge X-ray absorption spectra for 1.07% Zn/H-ZSM5 during various thermal treatments in H_2, He, or C_3H_8 (50 cm^3/g cat ∗ min, steady state).

near-edge spectrum changes. After mild thermal treatments, the *in situ* Zn/H-ZSM5 spectrum splits into two peaks (Fig. 4). These two peaks remain after cooling the Zn/H-ZSM5 sample to room temperature in flowing gas. A pulse of water introduced into the carrier gas restores the spectrum to that of fresh samples at room temperature. Thus, these hydration–dehydration processes are reversible and appear to reflect weak adsorption of water onto Zn species. The radial distribution function also shows an increased number of oxygen nearest neighbors consistent with water coordinated to Zn cations.

More severe thermal treatments (323–773 K) in He, H_2, or C_3H_8 lead to lower-intensity features in the near-edge region of dehydrated samples (Fig. 5), which reach a constant intensity at temperatures above 573 K. The intensity of these edge features decreases with temperature, but the Zn *K*-edge energy remains constant (9664 eV) during heating in He, H_2, or C_3H_8 (Fig. 5). Therefore, Zn species in Zn/H-ZSM5 remain as Zn^{2+} and do not reduce to Zn^0 during treatments in He or H_2, or during catalytic reactions of C_3H_8.

Zn/H-ZSM5 near-edge spectra do not resemble any of the available Zn standards (Fig. 6). After dehydration, edge features in Zn/H-ZSM5 begin to resemble Zn^{2+} species in ZnO/Al_2O_3 and ZnO/SiO_2 samples.

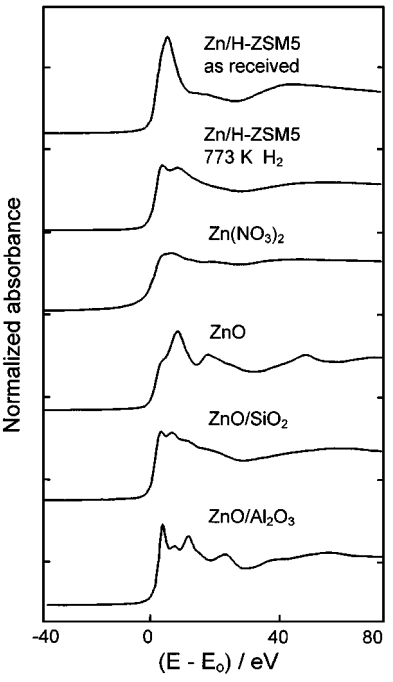

FIG. 6. Zn *K*-edge X-ray absorption near-edge spectra for 1.07% Zn/H-ZSM5, $Zn(NO_3)_2$, ZnO, Zn foil, ZnO/SiO_2, and ZnO/Al_2O_3 (all standards at 293 K in flowing H_2, 50 cm^3/g cat ∗ min).

3.3. X-ray Absorption Extended Fine Structure (EXAFS)

The extended fine structure in X-ray absorption spectra (EXAFS) reflects the scattering of ejected electrons by atoms near the absorber (21). The fine-structure region (>50 eV above the edge) contains information on the chemical identity and location (bond distances) of atoms near the absorber (22). Thus, it provides local structural information that complements the coordination symmetry features detected in the near-edge region.

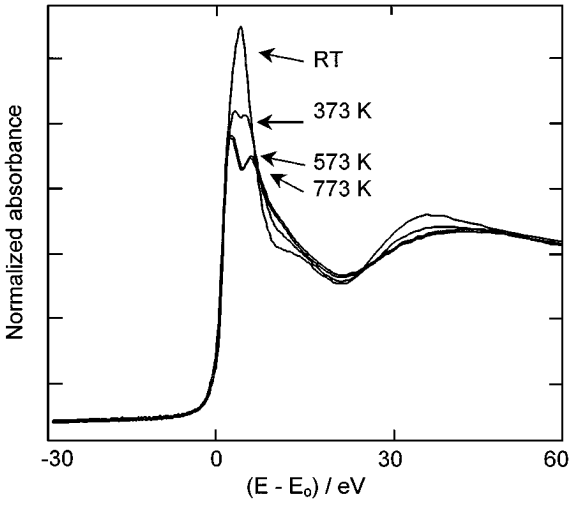

FIG. 5. Zn *K*-edge X-ray absorption near-edge spectra for 1.07% Zn/H-ZSM5 at RT, 373 K, 573 K, and 773 K in flowing H_2 (50 cm^3/g cat ∗ min, steady state).

EXAFS measurements at the Zn *K*-edge were analyzed using ZnO and Zn foil as standards to detect the presence of Zn–O, Zn–O–Zn, and Zn–Zn species. Room temperature spectra of fresh Zn/H-ZSM5, ZnO, and Zn foil result in the radial distribution functions shown in Fig. 7. The peak at 1.5 Å in ZnO reflects the presence of oxygen nearest neighbors. Zn atoms in bulk ZnO are present in tetrahedral structures with Zn–O distances of 1.95 Å (23). Peaks in the EXAFS radial distributions appear at a distance shorter than true interatomic distances because the distance measured is the actual distance between electron clouds, which is smaller than the distance between nuclei. Thus, the 1.5-Å peak in the radial distribution function corresponds to a true Zn–O bond length of 1.95 Å. A peak at 1.6 Å, similar to that in ZnO, is also present in the radial distribution function of fresh Zn/H-ZSM5, indicating the presence of Zn–O nearest neighbors. This peak in the Zn/H-ZSM5 spectrum, however, is significantly higher in magnitude than in the zinc oxide spectrum. The number of oxygen nearest neighbors giving rise to this peak was calculated by fitting the back Fourier transforms of the Zn/H-ZSM5 spectrum in Fig. 7. Standard data for the fit were generated by FEFF software (Version 6.01). The fit indicates that each Zn atom in fresh Zn/H-ZSM5 has 5.4 oxygen nearest neighbors at a bond distance of 2.09 Å.

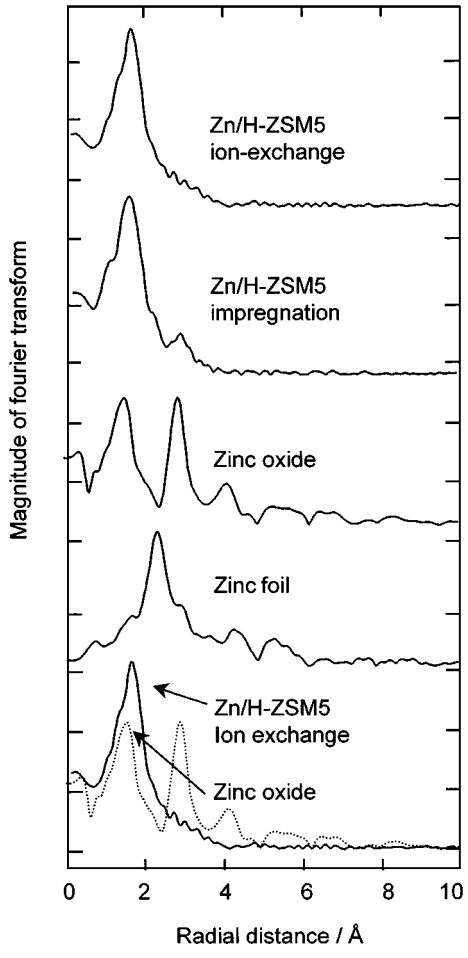

FIG. 7. EXAFS Zn *K*-edge radial distribution functions for fresh 1.07% Zn/H-ZSM5 (ion-exchange), 2.80% Zn/H-ZSM5 (impregnation), ZnO, and Zn foil.

Zn/H-ZSM5 fine-structure spectra do not contain a peak at 2.3 Å, which corresponds to Zn–Zn nearest neighbors in Zn foil, or a peak at 3.0 Å corresponding to Zn–Zn next nearest neighbors in ZnO (Fig. 7). This suggests that the Zn in Zn/H-ZSM5 is not present as ZnO crystallites, but as isolated Zn species with no Zn next-nearest neighbors. They are most likely at cation exchange positions inside the zeolite channels. Zeolitic Al and Si atoms do not appear as Zn neighbors in the fine structure because of unconstrained vibrations at surface cation exchange sites. EXAFS signals are sensitive to the degree of order around individual interatomic distances; atoms with broad distributions around their mean distance do not contribute strongly to the scattering spectrum (21,22).

Zn/H-ZSM5 samples synthesized by impregnation, instead of ion exchange, contain both exchanged Zn cations and external ZnO crystallites, which can be detected as Zn–Zn next nearest neighbors in the radial distribution function. Unlike ion-exchanged samples, the radial distribution function of Zn/H-ZSM5 prepared by impregnation shows a peak at 3 Å, similar to that for Zn next nearest neighbors in bulk ZnO (Fig. 7). Catalytic studies during propane conversion showed that Zn/H-ZSM5 prepared from ion-exchange methods are more active than those from impregnation techniques, but give identical product distributions at similar propane conversion levels (Table 3). These X-ray absorption data suggest that impregnation techniques lead to the formation of ZnO crystallites, which have been shown to be inactive for butane conversion (24) and which reduce to Zn metal and vaporize during propane reactions at 973 K.

TABLE 3

Propane Turnover Rates and Product Selectivity on Ion-Exchanged (1.30%) and Impregnated (2.80%) Zn/H-ZSM5 (773 K, 26.6 kPa C_3H_8, 74.7 kPa He, 8.1–8.3% Propane Conversion)

	Propane conversion turnover rate per Al site (10^{-3} s^{-1})	Product selectivities	
		Aromatics (C_6^+)	C_1–C_2
Ion-exchanged Zn/H-ZSM5	5.1	35.4	24.9
Impregnated Zn/H-ZSM5	2.0	33.6	25.8

A comparison of the radial distribution functions of fresh Zn/H-ZSM5 and Zn/H-ZSM5 treated in He at 773 K shows that the peak at 1.6 Å decreases in intensity after this treatment. The number of Zn nearest neighbors decreases from 5.4 to the value of 4.1 expected for tetrahedral Zn centers also found in ZnO (Fig. 8). This suggests that the fresh Zn/H-ZSM5 sample has water coordinated to the Zn species

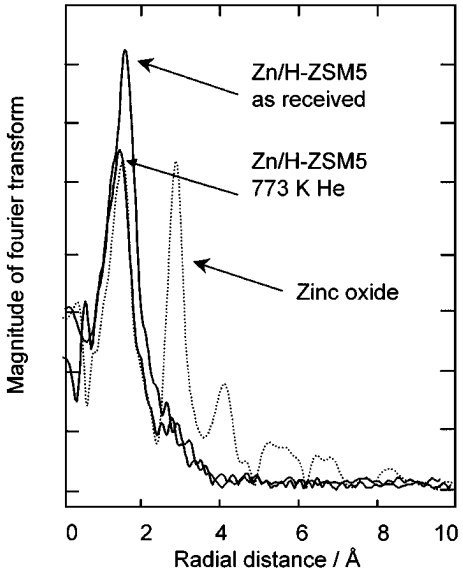

FIG. 8. Comparison of the EXAFS Zn *K*-edge radial distribution functions for fresh 1.07% Zn/H-ZSM5, 1.07% Zn/H-ZSM5 at 773 K, and ZnO (all samples are treated in flowing He, 50 cm^3/g cat $*$ min).

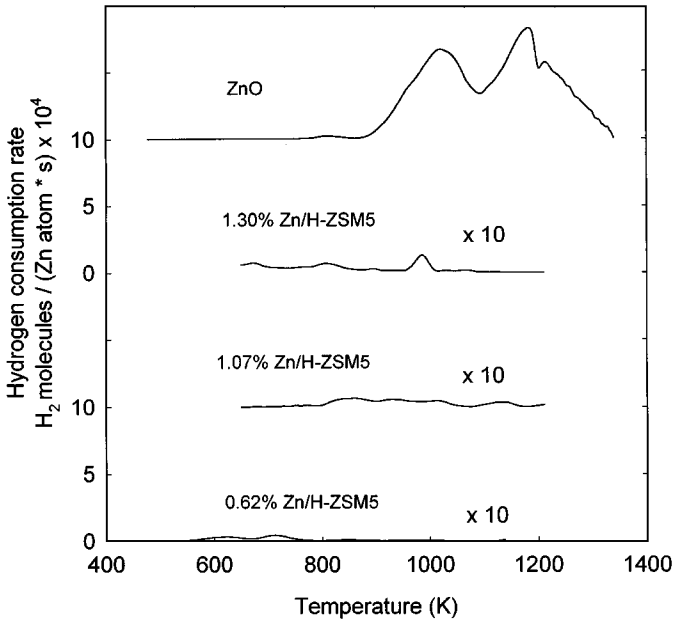

FIG. 9. Temperature-programmed reduction of ZnO and Zn/H-ZSM5 (80 cm^3/min, 20% H_2/Ar, 10 K/min, all samples from ion exchange).

and that this weakly bonded water is removed by thermal treatments. After dehydration at 773 K, Zn^{2+} cations reside in tetrahedral structures and do not show a significant number of next nearest neighbors.

3.4. Temperature-Programmed Reduction

Bulk oxide crystallites, when present, can also be detected by temperature-programmed reduction (TPR). TPR studies on bulk ZnO show that ZnO crystals begin to reduce to Zn metal and sublime around 850 K in flowing hydrogen. In contrast, Zn^{2+} cations in ion-exchanged Zn/H-ZSM5 samples (0.62 and 1.07 wt%) do not reduce even at 1150 K (Fig. 9). TPR studies on 1.30% Zn/H-ZSM5 show a slight reduction, suggesting that the zeolite contains a small amount of extracrystalline ZnO. The extent of reduction corresponds to less than 1% of the Zn cations in this sample.

In agreement with the X-ray absorption results described previously, TPR studies also show that impregnation techniques lead to the formation of extracrystalline ZnO. These extracrystalline ZnO species reduce at about 850 K, as also observed for bulk ZnO (Fig. 10). Bulk ZnO is completely reduced to Zn metal (H_2/Zn ratio of 0.99), while impregnated Zn/H-ZSM5 leads to a 0.46 H_2/Zn ratio, because about 54% of the Zn is present at cation exchange sites and not reducible, and 46% is present as reducible ZnO crystallites. In contrast with exchanged Zn species, these bulk ZnO crystals reduce and elute from the bed as Zn vapor in reducing environments, such as those present during propane reactions on Zn/H-ZSM5. It appears that properly prepared Zn/H-ZSM5 samples do not lose Zn by vaporization during catalysis.

3.5. Transformation of Zn into Active Zn Species during High-Temperature Treatment

Structural zeolitic studies of several M^{2+} cations (i.e., Cu, Mg) prepared by ion exchange from aqueous solution suggest that cationic species are initially present in zeolites as $(M^{2+}OH)^+$ (25). Berndt *et al.* (16) have shown that these $(M^{2+}OH)^+$ are also present in 1.5% Zn/H-ZSM5 (Si/Al = 23) samples. They detected equimolar amounts of CO_2 and H_2 when samples were treated in CO at high temperatures (>673 K) and suggested that this equimolar distribution results from CO interacting with a $(ZnOH)^+$ species and a neighboring H^+.

However, our X-ray absorption data show that $(ZnOH)^+$ species are not thermally stable and that they undergo dehydration, by coupling of $(ZnOH)^+$ species with acidic OH groups to form water and a bridging Zn^{+2} cation,

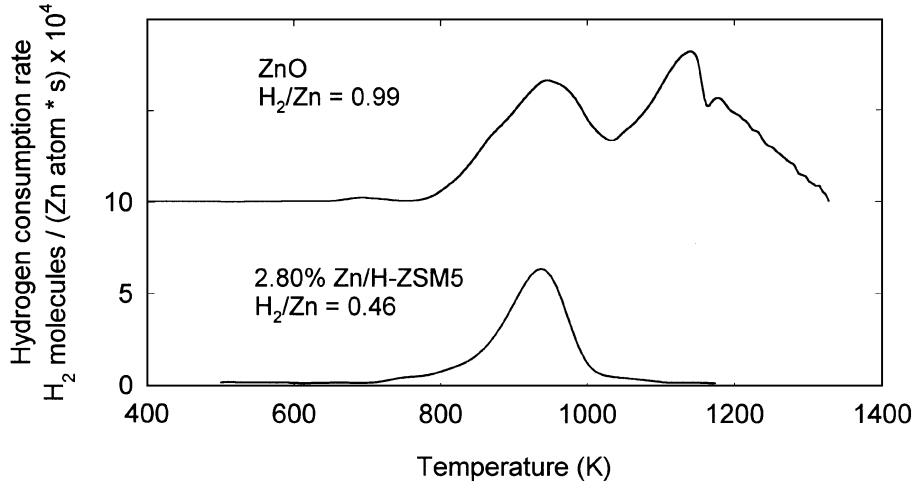

FIG. 10. Temperature-programmed reduction of ZnO and 2.80% Zn/H-ZSM5 (impregnated) (80 cm^3/min, 20% H_2/Ar, 10 K/min).

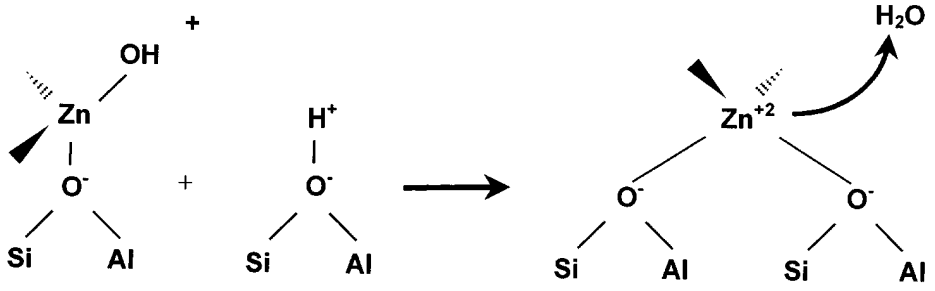

SCHEME 1. Dehydration of $(ZnOH)^+$ with a nearby proton to form H_2O and Zn^{2+} interacting with two cation-exchange sites.

interacting with two aluminum sites (Scheme 1). At high Zn^{+2} concentrations, dehydration may also occur by coupling of two $(ZnOH)^+$ species to form water and two Zn^{+2} cations bridged by oxygen (Scheme 2). The results of Berndt *et al.* (16) can then be explained by coupling of $(ZnOH)^+$ with OH groups at high temperatures. In the presence of CO, the desorbed water undergoes a water–gas shift reaction with CO to form the observed CO_2 and H_2 products.

3.6. Titration of Brønsted and Lewis Acid Sites with Ammonia

The density of Brønsted acid sites on H-ZSM5 and Zn/H-ZSM5 sample was measured by temperature-programmed desorption of preadsorbed ammonia. After ruling out the presence of ZnO crystallites in Zn/H-ZSM5 using X-ray absorption and TPR methods and suggesting that $(ZnOH)^+$ decompose by dehydration at high temperatures, the most probable active Zn^{2+} structures are shown in Scheme 3. One method to distinguish these two Zn species in propane conversion catalysts is to titrate residual H^+ species in Zn/H-ZSM5 using a basic molecule. However, when Zn replaces protons in H-ZSM5, it forms a Lewis acid site (Zn^{2+} cation) and ammonia then adsorbs on both Lewis and Brønsted acid sites. If Zn species I (Scheme 3) are present, the introduction of two Zn^{2+} would replace two H^+, resulting in one Zn^{2+} per Al site; this situation would lead to an NH_3/Al uptake similar to that on H-ZSM5. In contrast, if Zn species II (Scheme 3) are present, the introduction of one Zn^{2+} replaces two H^+, resulting in one Zn^{2+} per two Al sites and an NH_3/Al uptake that is less than the total amount of ammonia adsorbed on H-ZSM5 which depends on the number of Zn^{2+} cations in the sample.

On H-ZSM5, 0.96 NH_3 molecule was adsorbed per Al site, consistent with the expected presence of one H^+ per Al site (Table 4). Ammonia adsorption measurements indicate that the introduction of Zn species into ZSM5 channels for three Zn/H-ZSM5 samples with different Zn weight loadings (0.62, 1.07, and 1.30%) all lead to a decrease in the NH_3 uptake (compared with H-ZSM5). The ratio of NH_3 molecules adsorbed to Al sites decreases with increasing Zn loading (Table 4). NH_3 uptakes agree with those expected from the presence of species II (H-ZSM5 uptake—Zn/Al). These NH_3 data show that active Zn species in Zn/H-ZSM5 consist of Zn^{2+} cations interacting with two Al sites. This structure is similar to those reported by Yakerson *et al.* (18) after conducting pyridine adsorption studies on Zn/H-ZSM5.

3.7. Isotopic Titration of Brønsted Acid Sites with Deuterium

Because ammonia titrants interact with both Lewis and Brønsted acid sites in Zn/H-ZSM5 (26–28), the isotopic exchange of D_2 with surface hydrogens was used to measure the number of protons remaining after Zn exchange

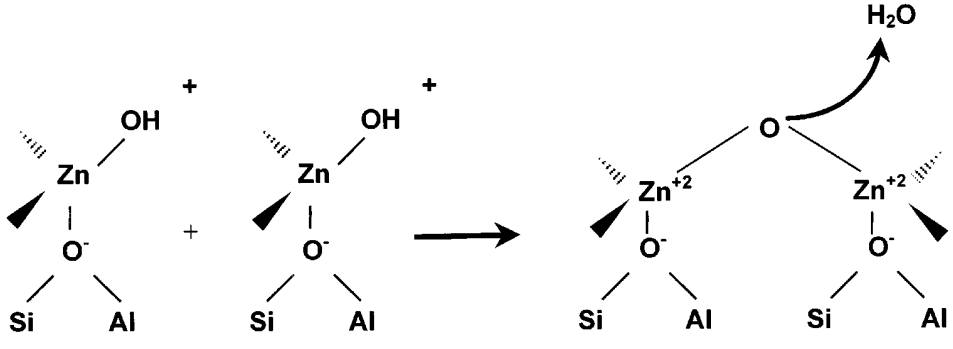

SCHEME 2. Dehydration of $(ZnOH)^+$ with another $(ZnOH)^+$ to form H_2O and two Zn^{2+} cations bridged by an oxygen.

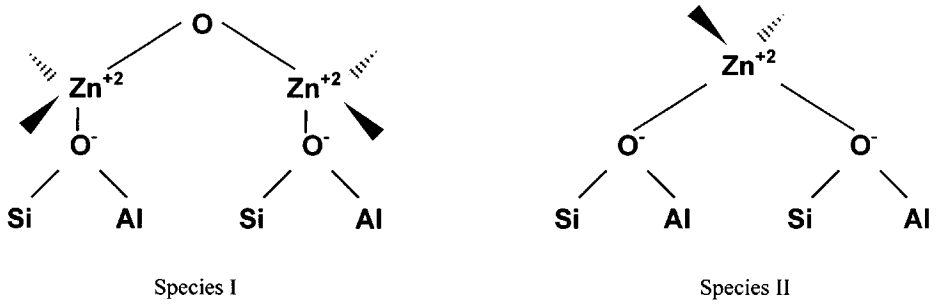

SCHEME 3. Possible active Zn species in Zn/H-ZSM5.

(29–33). Isotopic exchange experiments using D_2 were conducted on H-ZSM5 and on 1.30% Zn/H-ZSM5 by flowing D_2 over these samples and increasing the temperature. The number of hydrogen atoms desorbed as H_2 or HD was measured by mass spectrometry. Novakova *et al.* (33) used infrared spectroscopy to show that during isotopic exchange with D_2, deuterium replaces both protons and silanols in Y zeolite. Thus, the number of surface H atoms equals the number of Brønsted acid sites, as long as silanol groups are minority species.

On H-ZSM5, D_2 dissociates and exchanges with surface hydrogen atoms between 600 and 1000 K (Fig. 11). Surface H atoms desorb from the surface as HD and H_2. These HD and H_2 peaks account for the desorption of 1.04 H atoms per Al atom, consistent with the expected presence of one H^+ per Al site (Table 5). An independent calculation of the hydrogen surface concentration, based on the disappearance of D_2 rather than on the amount of hydrogen desorbed, leads to a similar value (1.09 D atoms per Al atom). The change in the gas-phase concentration of D_2 was less than 15% in all experiments. As a result, calculations based on D_2 consumption are less accurate that those based on the appearance of H_2 and HD. Desorption as HD accounted for 84% of the total hydrogens desorbed. The amount of H_2 produced is consistent with the amount expected from readsorption of the HD, suggesting that H_2 is formed primarily from readsorption of HD and subsequent exchange with remaining H^+ species. A prexponential factor and activation energy for this isotopic titration on H-ZSM5 were determined by fitting the HD desorption peak. The shape of this desorption peak is consistent with first-order kinetics and with an activation energy of 88 kJ/mol and a prexponential factor of 4.16×10^8 cm^3/(Al site $*$ s) (Fig. 11).

D_2–OH exchange on 1.30% Zn/H-ZSM5 (Zn/Al = 0.19) occurs at lower temperatures (400–600 K) than on H-ZSM5 (600–1000 K) (Figs. 11 and 12). This large difference in desorption temperatures indicates that hydrogen migration on ZSM5 surfaces is facile at these temperatures and the rate-determining step for the isotopic titration on H-ZSM5 is the dissociation of D_2, which is catalyzed by Zn^{2+} cations. These results are consistent with the proposed role of Zn^{2+} cations as "portholes" for hydrogen recombination, which results in higher aromatic site-time yields during propane reactions.

A prexponential factor and activation energy for the deuterium isotopic exchange on Zn/H-ZSM5 were determined by fitting the HD desorption peak with first-order kinetics. The calculated activation energy is 62 kJ/mol and the

TABLE 4

Total Amount of NH_3 Molecules Desorbed per Aluminum Site in H-ZSM5 and Zn/H-ZSM5 (NH_3 Adsorbed at 383 K, He Purge at 383 K for 3 h, 15 K/min, 100 cm^3/min)

		NH_3 adsorbed (NH_3 molecule/Al site)		
		Predicted		
Sample	Zn/Al	Species I	Species II	Experimental
H-ZSM5	—	—	—	0.96
0.62% Zn/H-ZSM5	0.10	0.96	0.86	0.84
1.07% Zn/H-ZSM5	0.16	0.96	0.80	0.78
1.30% Zn/H-ZSM5	0.19	0.96	0.77	0.74

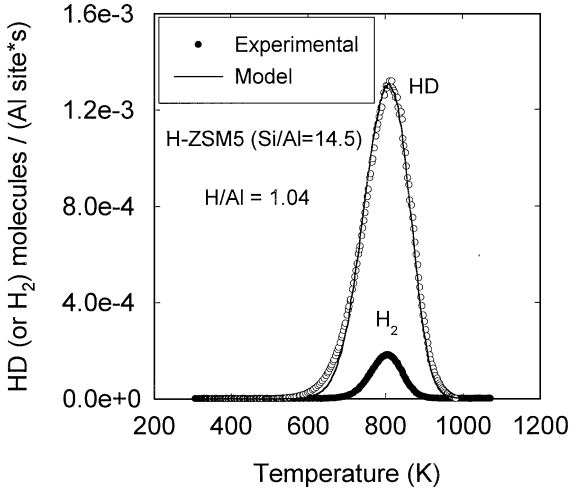

FIG. 11. Moles of HD and H_2 desorbed as a function of temperature during isotopic titration of Brønsted acid sites with D_2 on H-ZSM5. First-order kinetics give an activation energy of 88 kJ mol^{-1} (5% D_2/Ar, 80 cm^3/min, 10 K/min).

TABLE 5

Total Amount of H (D) Atoms Desorbed per Aluminum Site on H-ZSM5 and 1.30% Zn/H-ZSM5 [5% H_2/Ar (80 cm^3/min), pretreated at 773 K for 2 h, 5% D_2/Ar (80 cm^3/min), 10 K/min]

Sample	Zn/Al	Experimental (H atoms/Al site) or (D atoms/Al site)	
		Hydrogen balance	Deuterium balance
H-ZSM5	—	1.04	1.09
1.30% Zn/H-ZSM5	0.19	0.63	0.61

prexponential factor is 8.95×10^6 $cm^3/(Al\ site * s)$ (Fig. 12). The total amount of H_2 desorbed from Zn/H-ZSM5 during isotopic exchange with gas-phase D_2 is consistent with the amount expected from readsorption of gas-phase HD. Zn^{2+} cations decrease the activation energy for the hydrogen dissociation step, which limits both the isotopic exchange rate and the rate of propane aromatization.

As on H-ZSM5, the H species on Zn/H-ZSM5 desorbed as HD and H_2 during isotopic exchange with gas-phase D_2. The number of H atoms desorbed from Zn/H-ZSM5, however, was much lower (0.63 H atom per Al site) than on H-ZSM5 (Table 5). Recalculation of hydrogen surface concentration based on the consumption of D_2 rather than hydrogen desorption leads to a value of 0.61 D atom per Al site. Calculations based on the Zn loading from elemental analysis suggest that the number of hydrogen atoms desorbed (0.63 H/Al site) is very similar to the value of 0.62 H^+/Al $[1 - 2 \times (Zn/Al)]$ obtained when Zn^{2+} titrates two protonic sites during ion exchange. This Zn species was also suggested by the NH_3 desorption experiments. Zn^{2+} cations interact with two Al sites (O^-–Zn^{2+}–O^-).

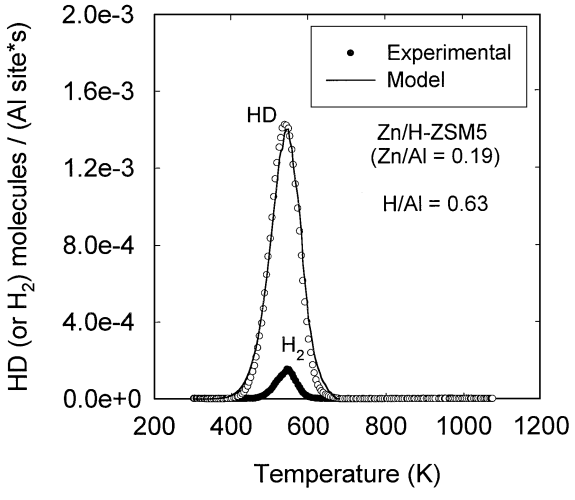

FIG. 12. Moles of HD and H_2 desorbed as a function of temperature during isotopic titration of Brønsted acid sites with D_2 on 1.30% Zn/H-ZSM5 (Zn/Al = 0.19). First-order kinetics give an activation energy of 62 kJ mol^{-1} (5% D_2/Ar, 80 cm^3/min, 10 K/min).

4. CONCLUSIONS

On H-ZSM5, propane converts to aromatic products with low selectivity and reacts predominantly to form undesired cracking products. Modifications of such pentasil zeolites with exchanged Zn cations increases the rate of hydrogen disposal, the propane turnover rate, and aromatic selectivity.

In situ Zn *K*-edge X-ray absorption studies have shown that Zn in Zn/H-ZSM5 (Si/Al = 14.5, ion exchange) is present as isolated Zn–O_x species, most likely located at zeolitic exchange sites, with about four oxygen nearest neighbors and without Zn next nearest neighbors. Temperature-programmed reduction studies indicate that reduction of bulk ZnO begins at 800 K, but Zn cations in Zn/H-ZSM5 catalysts do not reduce at temperatures exceeding 1173 K. These Zn ions remain as Zn^{2+} cations and do not reduce to zero-valent species during propane reactions at 773 K. Extracrystalline ZnO forms on samples prepared by impregnation techniques. These bulk ZnO crystals appear to be ineffective as catalysts for propane conversion. In contrast with exchanged Zn species, these bulk ZnO crystals reduce and elute from the bed as Zn vapor during propane reactions.

By analogy with other divalent metal cations, the most probable species from nitrate solution is $(ZnOH)^+$, but this Zn species is not thermally stable. On heating, Zn/H-ZSM5 undergoes dehydration. At low Zn loadings (<1.30 wt%), $(ZnOH)^+$ couples with a nearby OH group to form H_2O, which desorbs, and a Zn^{2+} cation. At high Zn loadings, $(ZnOH)^+$ may couple with another $(ZnOH)^+$ to form H_2O and two Zn^{2+} cations interacting with two Al sites and connected by bridging oxygen.

Ammonia adsorption measurements indicate that the introduction of Zn species into ZSM5 channels leads to a decrease in the amount of NH_3 adsorbed per Al site and is consistent with one Zn^{2+} cation replacing two protons and interacting with two Al sites. The isotopic titration of Brønsted acid sites with D_2 confirms these ammonia adsorption measurements. A decreased amount of hydrogen species is desorbed as HD and H_2 on Zn/H-ZSM5, when compared with H-ZSM5, indicating that Zn replaces protons during synthesis. Calculations based on the Zn loading from elemental analysis suggest that the number of hydrogen atoms desorbed is in agreement with the theoretical value expected for Zn^{2+} interacting with two Al sites (O^-–Zn^{2+}–O^-).

ACKNOWLEDGMENTS

This work was supported by the National Science Foundation (CTS-96-13632) and by the University of California startup funds. X-ray absorption data were collected at Stanford Synchrotron Radiation Laboratory (SSRL), which is operated by the Department of Energy (DOE), Office of Basic Energy Sciences, under Contract DE-AC03-76SF00515. The authors acknowledge David Barton (University of California), Dr. Stacey

I. Zones (Chevron Research and Technology Co.), and Dr. Mingting Xu (Engelhard Corp.) for their helpful discussions and technical assistance.

REFERENCES

1. Kitagawa, H., Sendoda, Y., and Ono, Y., *J. Catal.* **101**, 12 (1986).
2. Shibata, M., Kitagawa, H., Sendoda, Y., and Ono, Y., *in* "Proceedings of the 7th International Zeolite Conference," p. 717. Elsevier, Tokyo, 1986.
3. Scurrell, M. S., *Appl. Catal.* **41**, 89 (1988).
4. Ono, Y., and Kanae, K., *J. Chem. Soc. Faraday Trans.* **87**, 663 (1991).
5. Shigeishi, R., Garforth, A., Harris, I., and Dwyer, J., *J. Catal.* **130**, 423 (1991).
6. Guisnet, M., Gnep, N. S., Aittaleb, D., and Doyemet, J. Y., *Appl. Catal.* **87**, 255 (1992).
7. Guisnet, M., Gnep, N. S., and Alario, F., *Appl. Catal.* **89**, 1 (1992).
8. Mole, T., Anderson, J. R., and Creer, G., *Appl. Catal.* **17**, 141 (1985).
9. Ono, Y., and Kanae, K., *J. Chem. Soc. Faraday Trans.* **87**, 669 (1991).
10. Iglesia, E., Baumgartner, J. E., and Meitzner, G. D., *in* "Proceedings of the 10th International Congress on Catalysis" (L. Guczi, F. Solymosi, and P. Tetenyi, Eds.), p. 2353. Akadémiai Kiadó, Budapest, 1992.
11. Roessner, F., Hagen, A., Mroczek, U., Karge, H. G., and Steinberg, K. H., *in* "Proceedings of the 10th International Congress on Catalysis" (L. Guczi, F. Solymosi, and P. Tetenyi, Eds.), p. 1707. Akadémiai Kiadó, Budapest, 1992.
12. Iglesia, E., and Baumgartner, J. E., *Catal. Lett.* **21**, 55 (1993).
13. Iglesia, E., and Baumgartner, J. E., *ACS Symp. Ser. Div. Petrol. Chem.* **38**, 746 (1993).
14. Biscardi, J. A., and Iglesia, E., *Catal. Today* **31**, 207 (1996).
15. Berndt, H., Lietz, G., Lucke, B., and Volter, J., *Appl. Catal.* **146**, 351 (1996).
16. Berndt, H., Lietz, G., and Volter, J., *Appl. Catal.* **146**, 365 (1996).
17. Iglesia, E., Baumgartner, J. E., and Price, G. L., *J. Catal.* **134**, 549 (1992).
18. Yakerson, V. I., Vasina, T. V., Lafer, L. I., Sytnyk, V. P., Dykh, G. L., Mokhov, A. V., Bragin, O. V., and Minachev, K. M., *Catal. Lett.* **3**, 339 (1989).
19. Clausen, B. S., Steffensen, G., Fabius, B., Villadsen, J., Feidenhans'l, R., and Topsoe, H., *J. Catal.* **132**, 524 (1991).
20. Kunzl, V., *Collect. Czech. Chem. Commun.* **4**, 213 (1932).
21. Lytle, F. W., Via, G. H., and Sinfelt, J. H., "Synchrotron Radiation Research," p. 401. Plenum, New York, 1980.
22. Lytle, F. W., *in* "Applications of Synchrotron Radiation." Gordon Breach, Beijing, 1988.
23. Slater, J. C., "Symmetry and Energy Bands in Crystals." Dover, New York, 1972.
24. Yao, J., le van Mao, R., and Dufresne, L., *Appl. Catal.* **65**, 175 (1990).
25. Valyon, J., and Hall, W. K., *J. Phys. Chem.* **97**, 7054 (1993).
26. Karge, H. G., *in* "Catalysis and Adsorption by Zeolites" (G. Ohlmann *et al.*, Eds.), p. 133. Elsevier, Amsterdam, 1991.
27. Farneth, W. E., and Gorte, R. J., *Chem. Rev.* **95**, 615 (1995).
28. Gorte, R. J., and Biaglow, A. I., *ACS Symp. Ser. Div. Petrol. Chem. Adv. FCC Conversion Catal.*, 381 (1996).
29. Hall, W. K., Leftin, H., Cheselske, F., and O'Reilly, D. E., *J. Catal.* **2**, 506 (1963).
30. Uytterhoeven, J., Christner, L., and Hall, W. K., *J. Phys. Chem.* **69**, 2117 (1965).
31. Minachev, K. M., Dmitriev, R. V., Isakov, Y. I., and Bronnikov, O. D., *Kinet. Katal.* **12**, 626 (1971).
32. Dmitriev, R. V., Steinberg, K. H., Detjuk, A. N., Hofmann, F., Bremer, H., and Minachev, K. M., *J. Catal.* **65**, 105 (1980).
33. Novakova, J., Kubelkova, L., and Jiru, P., *J. Chem. Soc. Faraday Trans.* **77**, 1331 (1981).